Identifying photoreceptors in blind eyes caused by *RPE65* mutations: Prerequisite for human gene therapy success

Samuel G. Jacobson*†, Tomas S. Aleman*, Artur V. Cideciyan*, Alexander Sumaroka*, Sharon B. Schwartz*, Elizabeth A. M. Windsor*, Elias I. Traboulsi‡, Elise Heon§, Steven J. Pittler¶, Ann H. Milam*, Albert M. Maguire*, Krzysztof Palczewski‖, Edwin M. Stone**, and Jean Bennett*

*Department of Ophthalmology, University of Pennsylvania, Philadelphia, PA 19104; ‡Cole Eye Institute, Cleveland Clinic Foundation, Cleveland, OH 44195; §Department of Ophthalmology and Vision Sciences, Hospital for Sick Children, Toronto, ON, Canada M5G 1X8; ¶Department of Physiological Optics, University of Alabama at Birmingham, Birmingham, AL 35294; ‖Department of Ophthalmology, University of Washington School of Medicine, Seattle, WA 98195; and **Howard Hughes Medical Institute and Department of Ophthalmology, University of Iowa Carver College of Medicine, Iowa City, IA 52242

Mutations in *RPE65*, a gene essential to normal operation of the visual (retinoid) cycle, cause the childhood blindness known as Leber congenital amaurosis (LCA). Retinal gene therapy restores vision to blind canine and murine models of LCA. Gene therapy in blind humans with LCA from *RPE65* mutations may also have potential for success but only if the retinal photoreceptor layer is intact, as in the early-disease stage-treated animals. Here, we use high-resolution *in vivo* microscopy to quantify photoreceptor layer thickness in the human disease to define the relationship of retinal structure to vision and determine the potential for gene therapy success. The normally cone photoreceptor-rich central retina and rod-rich regions were studied. Despite severely reduced cone vision, many *RPE65*-mutant retinas had near-normal central microstructure. Absent rod vision was associated with a detectable but thinned photoreceptor layer. We asked whether abnormally thinned *RPE65*-mutant retina with photoreceptor loss would respond to treatment. Gene therapy in *Rpe65*−/− mice at advanced-disease stages, a more faithful mimic of the humans we studied, showed success but only in animals with better-preserved photoreceptor structure. The results indicate that identifying and then targeting retinal locations with retained photoreceptors will be a prerequisite for successful gene therapy in humans with *RPE65* mutations and in other retinal degenerative disorders now moving from proof-of-concept studies toward clinical trials.

visual cycle | Leber congenital amaurosis | rod | cone | retinal imaging

Discovery of the molecular causes of blinding incurable retinal degenerative diseases has improved diagnosis and mechanistic understanding and provided the hope of gene-based therapies. One autosomal recessive human disease seems especially approachable with gene replacement therapy: the childhood-onset form of blindness known as Leber congenital amaurosis caused by mutations in the *RPE65* gene (1). *RPE65* encodes a 65-kDa protein located in the retinal pigment epithelium (RPE) and essential for vertebrate vision. *RPE65* mutations prevent the normal cycling of retinoids, leading to photoreceptors without light-sensitive visual pigment and eyes with blindness (1–8). Proof-of-concept studies using viral vector-mediated *RPE65* gene delivery to the eye have shown dramatic restoration of vision in a naturally occurring canine model (9, 10) and a murine knockout (11). Advance to human clinical trials would seem to be the logical next step.

Translation from laboratory to clinic of gene therapy for *RPE65*-associated Leber congenital amaurosis rests on the unproven assumption that the human disease shares a key feature with the canine and murine models. The *RPE65*-mutant dog and *Rpe65*−/− mouse show the unusual feature of dissociation of retinal structure and function. In most other retinal degenerations, loss of photoreceptor structure is the underlying basis for loss of photoreceptor function (12, 13). Both animal models of *RPE65* disease, however, retain photoreceptor structure despite severe visual impairment, and the gene therapy successes have occurred at disease stages when photoreceptor structure was still intact (9–11).

How can it be determined whether humans with this genetic blindness have photoreceptor structural integrity short of performing retinal biopsy (14) or examining rare postmortem donor tissue (15)? We used *in vivo* high-resolution microscopy and correlative measures of vision (16–18) in patients with *RPE65* mutations to determine the relationship of structure to function. Photoreceptor layer thickness and vision were quantified in regions normally rich in cones and rods. The finding of patches of thinned photoreceptor layer in human *RPE65* retinae led to a study of gene therapy in late-stage *Rpe65*−/− mice with photoreceptor loss. From these human and murine results emerge guidelines for conducting a gene therapy trial in humans with *RPE65* mutations.

Materials and Methods

Human Subjects. Of the 59 participating patients, 11 had *RPE65* mutations (Table 1). There were 48 patients (ages 9–68 years) with negative *RPE65* mutation screening (19) or X-linked or dominant retinitis pigmentosa. Normal subjects ($n = 21$, ages 19–58 years) were included. Informed consent was obtained, and procedures followed institutional guidelines and the Declaration of Helsinki.

Optical Coherence Tomography (OCT). Cross-sectional retinal reflectivity profiles were obtained with OCT (Humphrey Instruments, Dublin, CA) by using published techniques (16–18). In eight *RPE65* patients [all but patient 1 (P1), P2, and P11] and five normals, six scan groups were used to cover a 18×12-mm² region of the retina centered on the fovea at high lateral resolution. Each scan group covered a region of 6×6 mm² of retina by using 21 parallel horizontal ("raster") scans of 6-mm length, vertically separated by 0.3 mm (18). Postacquisition processing of OCT data was performed with custom programs (16–18). Spatial maps of retinal thickness were derived from the

NEUROSCIENCE

Table 1. *RPE65* mutations in Leber congenital amaurosis patients

Patient	Age, y	Gender	Mutations	Source*
P1	11	Male	Y368H/Y368H	17
P2	12	Female	97del20bp/97del20bp	5, 17, 35, 48
P3	18	Female	L341S/L341S	This study
P4	19	Female	R44Q/R91W	48
P5	20	Female	L343X	This study
P6	21	Male	E417Q/E417Q	48
P7	27	Female	H182R/H182R	This study
P8	28	Female	Y368H/297del1bp	This study
P9	40	Female	K303X/Y431C	49
P10	41	Male	Y144D/Y144D	48
P11	53	Male	IVS1 + 5G>A, homoallelic	35,48,50

*Previous report of genotype and/or phenotype.

groups of raster scans (18). Individual normal thickness maps were aligned for fovea and optic nerve to determine local statistics. Patient maps were aligned to normal maps and subtracted from the lower limit of normal (mean − 2 SD) to estimate retinal regions of significant thinning. Cross sections of scans are displayed after averaging two to five aligned scans and using a 2 × 1 moving median filter to reduce speckle noise in lateral dimension while keeping the original resolution in the longitudinal direction. The location of the outer nuclear layer (ONL) in cross-sectional scans was defined as the signal trough delimited by the signal peaks corresponding to the outer plexiform layer and outer limiting membrane. ONL thickness was defined in a semiautomated fashion between the samples representing the maximum slope on both sides of the signal trough (18).

Psychophysics. Dark-adapted thresholds were measured (at 2° intervals, 650- and 500-nm stimuli, 1.7° diameter, 200-ms duration) in the same retinal regions as OCT scans. Visual function techniques and analysis methods were as described (17, 18, 20).

Structure vs. Function. The relationship between photoreceptor structure and colocalized visual function was defined in patients by using ONL thickness and dark-adapted sensitivity. Patient results were compared with an idealized model of the expected relationship in pure photoreceptor degenerations. The model assumes that photoreceptor function is proportional to the product of the number of surviving photoreceptors and the length of their outer segments; both of these parameters are proportional to ONL thickness (13). Thus, to a first approximation, loss of light sensitivity (in linear units) would be expected to be proportional to the square of ONL thinning.

Murine Studies: Animals and Experimental Procedures. $Rpe65^{-/-}$ ($n = 82$) and WT ($n = 12$) mice of the same background (4) were raised in 12-h on/12-h off cyclic dim (<3 lux) light. Treatment group 1 (Tx1) of $Rpe65^{-/-}$ mice (ages 15–24 mo, $n = 25$) received unilateral subretinal injections of AAV2/1-CMV-*hRPE65* (11). Contralateral subretinal injections of buffered saline served as controls. Treatment group 2 (Tx2; ages 17–26 mo, $n = 24$) was given 9-*cis*-retinal by oral gavage (5). Electroretinograms (ERGs) were recorded ≈2 mo after subretinal injections ($n = 25$) and 48 h after oral cis-retinoid ($n = 21$); untreated $Rpe65^{-/-}$ mice (ages 3 mo, $n = 11$; 16–24 mo, $n = 12$) and WT mice (ages 3 mo, $n = 6$; 15–25 mo, $n = 6$) served as controls. Eyes were enucleated for morphometry (Tx1: $n = 5$; untreated $Rpe65^{-/-}$: $n = 7$; WT: $n = 3$) or retinoid analysis (Tx1: $n = 17$; Tx2: $n = 22$; untreated $Rpe65^{-/-}$: $n = 10$). Studies were in accordance with the Association for Research in Vision and Ophthalmology Statement for the Use of Animals in Ophthalmic and Vision Research and institutional review.

ERG. Details of our rodent ERG methods were as described (11, 21).

Histology. Eyes were enucleated and fixed in 4% paraformaldehyde and 0.5% glutaraldehyde in 0.1 M PBS. Samples were washed in PBS, dehydrated, and embedded in JB-4 resin (Polysciences). Serial sections (10 μm thick) along the vertical meridian were stained with Richardson's mixture of methylene blue and azure II and photographed. Images were scaled by using a calibration tool photographed under the same (×40) magnification. ONL thickness measurements were made at three locations separated 50 μm from each other and centered 1 mm from the optic nerve in superior retina. An average of three measurements provided a single value of ONL thickness for each retina.

Retinoid Analyses. All procedures related to extraction, derivatization, and separation of retinoids from dissected mouse eyes were as described (5, 22, 23). Each eye from treated animals was analyzed individually. The following criteria were used to define success in the unilateral subretinal AAV2/1-CMV-*hRPE65*-treated animals (Tx1): the peak area of *syn*-11-*cis*-retinal oxime was equal to or higher than 6 pmol, the peak elution for *syn*-11-*cis*-retinal oxime was eluted ±0.3 min from the authentic standard *syn*-11-*cis*-retinal oxime, and the untreated eyes did not have the *syn*-11-*cis*-retinal peak. The following criteria were used to define success in 9-*cis*-retinal-treated animals (Tx2): the chromatographic separation of retinoid yielded absorbance at 325 nm for a peak corresponding to *syn*-9-*cis*-retinal oxime >0.3 mAu, the results were comparable between two samples from the same animal, both *syn*- and *anti*-9-*cis*-retinal oximes were clearly separated, and the spectrum of syn-9-*cis*-retinal yielded a low noise spectrum for the identification of the retinoid.

Results

Retinal Thickness Topography in *RPE65*-Mutant Human Retinas. *En face* viewing is the traditional method of assessing retinal abnormality in the clinic. The advent of high-resolution depth (cross-sectional) imaging permits topographical maps of retinal thickness to be constructed and disease effects to be analyzed by this nontraditional metric (17, 18). As a step toward understanding disease severity in human *RPE65* mutations, we compared the retinal thickness topography of the patients with that of normal subjects (Fig. 1, *en face* views, *Upper Insets*). The retina of a normal subject (age 22) has a central depression or foveal pit, a surrounding ring of increased thickness with displaced inner retinal layers from foveal formation, then, a decline in thickness with distance from the fovea and a prominent crescent-shaped thickening extending into superior and inferior poles of the optic nerve, attributable to the converging axons from ganglion cells (Fig. 1*A*). The calculated lower limit of normal thickness is also shown (Fig. 1*A Lower Inset*).

Retinal topography in a 20-year-old with *RPE65* mutations, P5 (Fig. 1*B*), appears similar to normal. A retinal thickness difference map (Fig. 1*B Lower Inset*) relates this *RPE65*-mutant retina to the lower limit of normal and confirms that there are no areas of reduced thickness. P4 (age 19) also has a normal retinal thickness map (data not shown). A 21-year-old, P6 (Fig. 1*C*), retains topographical detail but the retina is thinned compared with normal. The difference map highlights regions of significantly reduced thickness; most prominent thinning is in a region ≈1–3 mm from the preserved central island. P7, a 27-year-old, shows retinal thinning that is more widespread and extends into the temporal retina (Fig. 1*D*). P9 and P10, ages 40 and 41, respectively, show differences in retinal topography (Fig. 1 *E* and *F*). P9 has more central retinal preservation of thickness than P10. The *en face* images in these patients also differ; an atrophic lesion surrounds the fovea in P10 but not in P9. P8, at age 28, has similar topographical and difference maps (data not shown) to those of P9. A range of thickness topographies, suggesting a range of severities of retinal

Fig. 1. *RPE65*-mutant human retinas with normal thickness topography or localized retinal thinning. Topographical maps from high-resolution depth imaging of the central retina in a normal subject, age 22 (*A*), and five patients with *RPE65* mutations (ages 20–41) (*B–F*). (*Insets Upper Right*) *En face* images. (*A Inset Lower Right*) The lower limit (mean − 2 SD) of normal. (*B–F Insets Lower Right*) A difference map (subtracted from normal lower limit) showing regions of thinned retina (gray). All images are depicted as left eyes. ON, optic nerve. F, fovea. N, nasal, T, temporal, S, superior, I, inferior.

Fig. 2. Photoreceptor nuclear layer in *RPE65*-mutant retinas. (*A–D*) Cross-sectional retinal images along the horizontal (*Left*) and vertical (*Right*) meridia through the fovea in a normal subject (*A*) and three patients with *RPE65* mutations (*B–D*). ONL is indicated to the left of the images. (*E*) ONL thickness across horizontal (*Left*) and vertical (*Right*) meridia in normal subjects and patients with *RPE65* mutations. Normal ONL thickness mean (thin line) and ±2 SD (gray) are indicated.

degeneration, thus exists among adults with *RPE65* mutations and there is no simple relationship of age and retinal thickness.

Photoreceptor Layer Is Definable in Adults with *RPE65* Mutations. Morphometry of the photoreceptors or ONL as thickness or cell numbers has classically been used to assay retinal phenotype in animal retinal degenerations (24, 25). Such histopathological data have not been available for human retinopathies except from postmortem donor tissue (12). Human ONL thickness has recently become measurable *in vivo* by high-resolution optical cross-sectional imaging (17, 18). We quantified ONL thickness along horizontal and vertical meridia in normal and *RPE65*-mutant retinas (Fig. 2). The normal human retina in cross section has discernible laminae (Fig. 2*A*). At the cone-rich fovea, a reflectance marks the vitreoretinal interface, a drop in reflectivity marks the ONL, and deeper reflections correspond to photoreceptor inner and outer segments and RPE. Temporal to the fovea in the horizontal meridian (Fig. 2*A Left*) and also in the vertical meridian (Fig. 2*A Right*), total retinal thickness increases and inner retinal laminae are prominent. At further eccentricities, thickness gradually tapers. In the vertical meridian, in addition to neural and synaptic laminae, ganglion cell axons traverse superficially to converge and exit at the optic nerve. From the fovea into the peripheral retina, the ONL normally declines in thickness.

RPE65 mutant retinas also show an identifiable photoreceptor lamina in cross section (Fig. 2 *B–D*). The foveas of P4 and P6 have normal ONL thickness, but P7 has abnormally reduced thickness. Eccentric to the fovea, P4 and P6 show a more pronounced decline in ONL thickness than normal. The ONL in P4 is detectable and appears relatively constant in thickness across horizontal and vertical meridia, but P6 shows an increase in ONL thickness between ≈3 and 6 mm in both temporal and superior retinal sections. At greater eccentricities in the tempo-

ral retina, there is a decline in ONL thickness and it is not visible at more superior retinal eccentricities. In P7, the ONL is not evident beyond the very central retina.

Photoreceptor layer thickness for normal subjects and the 11 *RPE65*-mutant retinas was analyzed in horizontal (temporal) and vertical (superior) meridia (Fig. 2*E*). At the fovea, there was measurable ONL in all *RPE65*-mutant retinas and nearly half had normal thickness. Immediately adjacent to the fovea, there was abnormally reduced ONL and in many it was not detectable. An increase in ONL thickness in the superior retina between ≈3 and 6 mm from the fovea was evident in three retinas (P2, P4, and P6). P6 also showed this increase in temporal retina (Fig. 2*E*).

***RPE65*-Mutant Retinas Have Greater Photoreceptor Layer Thickness than Predicted for Amount of Visual Loss.** The relationship between photoreceptor nuclear layer structure and visual function was examined in *RPE65*-mutant retinas at selected locations known to have the highest densities of cones or rods in normal retinas (26). Comparisons were made with normal subjects and other retinal degenerations not caused by *RPE65* mutations (Fig. 3). At the fovea, average normal peak cone density is ≈200,000 cells·mm^{-2} (26) and foveal ONL thickness in normal subjects averages 97 μm (SD = 17 μm, $n = 15$, age = 19–56). In non-*RPE65* patients, foveal ONL thickness reduction was predictably related to central visual function over a 3-log unit range from normal to severely abnormal vision (Fig. 3*A*). All 11 patients with *RPE65* mutations had abnormally reduced foveal cone vision; 5 of 11 had no measurable dark-adapted sensitivity. In 8 of 11, ONL thickness was greater than
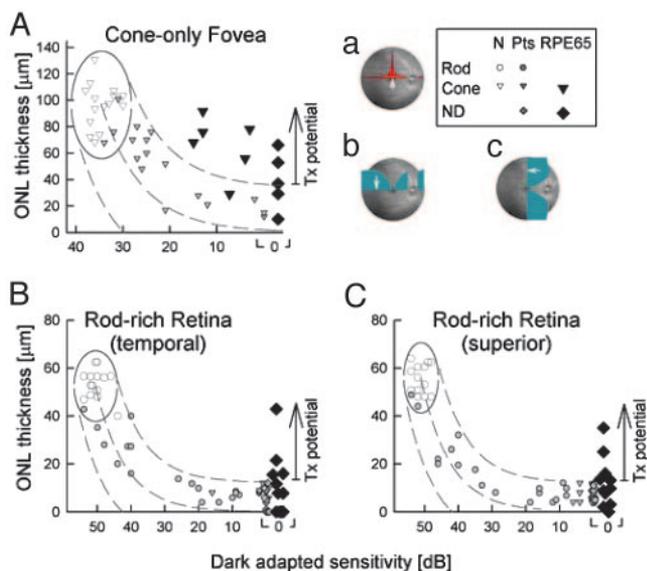
Fig. 3. *RPE65*-mutant human retinas can have more photoreceptor nuclear layer than predicted from vision. (*A*) Foveal ONL thickness as a function of dark-adapted cone-mediated sensitivity (650 nm). (*B* and *C*) ONL thickness as a function of dark-adapted sensitivity (500 nm) at 3.6 mm in temporal (*B*) and superior (*C*) retina. Rod, rod-mediated sensitivity; Cone, cone-mediated sensitivity; Pts, patients without *RPE65* mutations. Normal variability is described by the ellipses encircling the 95% confidence interval of a bivariate Gaussian distribution. Dotted lines define the idealized model of the relationship between structure and function in pure photoreceptor degenerations and the region of uncertainty that results by translating the normal variability along the idealized model. The region encompassing data with greater than expected ONL thickness is marked as treatment (Tx) potential. (*Inset*) Retinal location (white arrow on fundus image) of colocalized measures of structure and function. Overlaid onto the fundus image are cone density (*a*) and rod density (*b* and *c*) along horizontal and vertical meridia (26).

expected for the level of dysfunction; in 5 individuals, ONL was within normal limits. The relationship of function and structure in three patients with *RPE65* mutations was not distinguishable from that of non-*RPE65* patients.

Two rod-rich regions analyzed were at 3.6 mm eccentric to the fovea. At 3.6 mm temporal to the fovea, rod photoreceptor density normally peaks at ≈140,000 cells·mm^{-2} and the rod/cone ratio is 20:1 (26). Normal ONL thickness at this location averages 53 μm (SD = 6 μm, n = 17, age = 19–56). The 3.6-mm superior location is theoretically within the 3- to 5-mm eccentricity of the rod ring "hot spot" in which the highest rod densities occur in normal human retina. Rod densities in this region normally average 160,000 cells·mm^{-2} and the rod/cone ratio is ≈25:1 (26). Normal ONL thickness at this locus averages 56 μm (SD = 6 μm, n = 14, age = 19–56).

In non-*RPE65* patients, ONL thickness reduction at the rod-rich retinal loci was predictably related to dark-adapted vision over a 5-log unit range from normal to severely abnormal (Fig. 3 *B* and *C*). No vision was measurable in all 11 individuals with *RPE65* mutations at these loci. At the temporal location, 4 of 11, and at the superior location 5 of 11 *RPE65*-mutant retinas showed a significantly greater amount of ONL thickness preservation for this severity of visual loss.

Rpe65$^{-/-}$ Mice at Late-Disease Stages Can Show Visual Restoration by Gene Therapy.
Given the evidence for abnormally reduced ONL thickness (particularly outside the fovea) in many humans with *RPE65* mutations, we asked whether restoration of vision would be possible at disease stages with significant photoreceptor degeneration. To begin to answer this question, results of gene
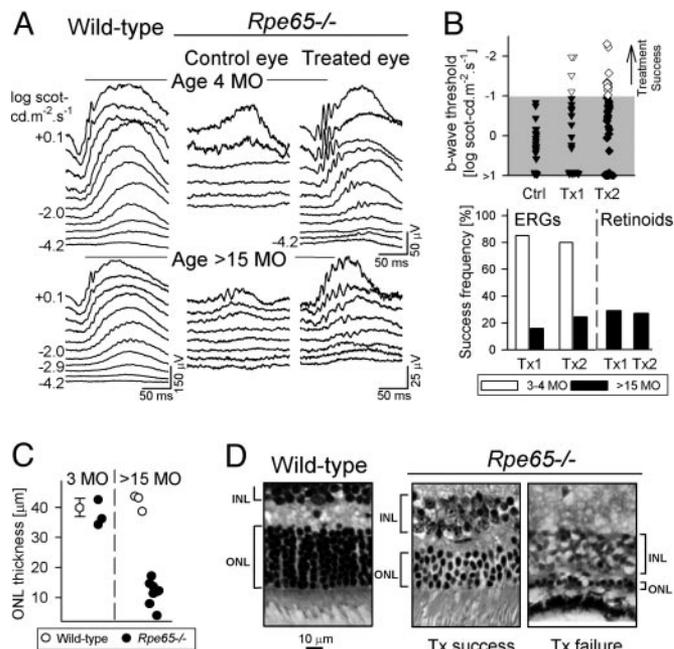
Fig. 4. Gene therapy in *Rpe65*$^{-/-}$ mice at advanced disease stages leads to limited visual restoration. (*A*) Comparison of ERGs in young (4 mo) and old (>15 mo) WT (*Left*) and *Rpe65*$^{-/-}$ mice (*Center* and *Right*). (*Center*) Saline-injected control eyes of *Rpe65*$^{-/-}$ mice illustrate the severe ERG abnormality. (*Right*) The AAV2/1-CMV-*hRPE65*-treated eyes show visual restoration. Stimulus onset is at trace onset; stimulus luminance is at left of traces. (*B*) Summary of treatment results. ERG thresholds in >15-mo-old *Rpe65*$^{-/-}$ mice after treatment with AAV2/1-CMV-*hRPE65* (Tx1) or oral 9-*cis* retinal (Tx2) are compared with saline-injected (Ctrl) eyes. Unfilled symbols (treatment success) are results falling beyond the 99% confidence interval limit (upper boundary of gray) determined from uninjected, age-matched, *Rpe65*$^{-/-}$ mice. Frequency of treatment success by ERG and retinoid biochemistry for Tx1 and Tx2 in young (empty bars) versus old (filled bars) *Rpe65*$^{-/-}$ mice is shown. (*C*) ONL thickness (1 mm superior to optic nerve) in 3-mo-old vs. 24-mo-old *Rpe65*$^{-/-}$ mice (●) is compared with age-matched WT (○) mice. ONL thickness data (mean ± 2 SD) for young WT mice (25) is shown. (*D*) Retinal histological sections (1 mm superior to optic nerve) from an old WT mouse (*Left*) are compared with two old *Rpe65*$^{-/-}$ mice treated with gene therapy: one with ERG success (*Center*) and one with failure (*Right*). The ONL and the inner nuclear layer (INL) are indicated by brackets.

therapy would need to be studied in an *RPE65*-mutant animal with considerable photoreceptor loss. Natural history data in *Rpe65*$^{-/-}$ mice indicate there is degeneration that progresses to severe photoreceptor loss by 18–24 mo (27). We maintained *Rpe65*$^{-/-}$ mice until older ages and treated them with subretinal gene therapy; success rates for visual restoration at late- and early-disease stages were then compared (11).

Retinal function in 3- to 4-mo-old *Rpe65*$^{-/-}$ mice is severely abnormal: ERG thresholds are greatly elevated, requiring ≈4 log units brighter stimuli to elicit responses than in WT mice (Fig. 4*A*). Gene therapy with AAV2/1-CMV-*hRPE65* in *Rpe65*$^{-/-}$ mice at ages 1–2.5 mo is ≈80% successful by ERG assay 2 mo later (11). A representative example of a therapeutic success (treated at 2 mo, evaluated at 4 mo) shows dramatically improved function with near-normal thresholds in the treated eye, compared with the contralateral saline-injected control eye. Gene therapy in *Rpe65*$^{-/-}$ mice at ages 17–24 mo (n = 25) was effective but in a far smaller percentage of eyes. Representative ERGs from a 17-mo-old mouse with therapeutic success show improved b-wave thresholds in the treated eye; the brightest stimuli, however, did not elicit certain waveform features (e.g., a-wave) typically seen in WT (see age-related normal) or treated younger *Rpe65*$^{-/-}$ mice (Fig. 4*A*).

B-wave thresholds in control eyes were compared with their contralateral-treated eyes (Fig. 4B, Ctrl vs. Tx1). Treatment success was defined as results falling beyond the 99% confidence interval limit (gray area) for b-wave threshold in uninjected, age-matched $Rpe65^{-/-}$ mice. Success occurred in 4 of 25 animals (16%). Thresholds in animals with a treatment effect were significantly better than those from uninjected, age-matched, $Rpe65^{-/-}$ (-1.65 ± 0.42 vs. $+0.47 \pm 1.45$ log scot-cd·m^{-2}·s^{-1}) mice ($P < 0.05$) and fall within the level of improvement we reported for young mice (11). The retinoid content was measured in treated eyes and saline-injected contralateral eyes from a subset of the older animals. Five of 17 treated eyes (29%) had clearly detectable 11-cis retinal; no measurable chromophore was found in saline-injected control eyes (Fig. 4B).

Was the reduced success of treatment in older versus younger mice (Fig. 4B Lower) possibly caused by subretinal surgical intervention in these eyes with advanced retinal degeneration? Oral 9-cis-retinal also successfully restores visual function in ≈80% of treated young $Rpe65^{-/-}$ mice (5, 28) and does not involve retinal surgery (Fig. 4B, Tx2). In a series of older mice (n = 21) of comparable ages to those used for gene therapy, oral 9-cis retinal was administered and ERGs were studied 48 h later. These mice also had a lower success rate (24%) than younger counterparts (Fig. 4B Lower); the success rates with oral intervention versus gene therapy were not significantly different (P > 0.05). Analysis of retinoid biochemistry in 9-cis-retinal-fed animals (n = 22) indicated that treatment success rates were also low. Only 6 of 22 (27%) mice had significant accumulation of 9-cis-retinal, whereas the rest of the treated mice had trace amounts. Control (untreated) $Rpe65^{-/-}$ mice (n = 10) did not contain measurable 9-cis-retinal.

ONL thickness measurements in 3- and 17- to 24-mo-old $Rpe65^{-/-}$ mice (Fig. 4C; retinal locus is 1 mm superior to optic nerve) confirm previous data indicating that the ONL can be normal at early ages, but is reduced at later ages (27). In the older age group, the ONL could have three to four photoreceptor nuclei or be reduced to a single row, suggesting variability in the amount of degeneration. We had the opportunity to inquire in one of the gene therapy successes whether there was any difference in ONL thickness compared with eyes that failed to respond. Fig. 4D compares histological sections (at 1 mm superior to the optic nerve) taken from an older WT mouse and two treated $Rpe65^{-/-}$ mice. The eye with gene therapy treatment success shows about four rows of nuclei, compared with the treatment failure, which has only a single row of nuclei (similar severity was found in three other treatment failures). This morphological evidence supports the intuitive notion that retinas with higher numbers of retained photoreceptor cells (and intact RPE) are likely to have greater potential for treatment success.

Discussion

Restoration of vision is the ultimate goal of human retinal degeneration research. In vivo gene transfer to photoreceptor and RPE cells in animal models has led to dramatic results showing reversal of defective gene function or prevention of apoptotic cell death (9, 29–32). This success has heightened expectation that the ultimate goal is approachable in human eye disease. Specifically, for blindness caused by RPE65 mutations, large and small animal models have been treated successfully with gene transfer (9–11). Vision has been restored to blind animals that had mostly intact photoreceptors but lacked the 11-cis-retinal chromophore caused by an interrupted retinoid cycle in the RPE.

Humans with RPE65 deficiency have been suspicious for having complexity of disease mechanism: there is extremely reduced photoreceptor function and visual loss from early life, but there can be hallmarks of pigmentary degeneration and atrophy of the retina (2, 3, 33–40). The reduced vision is consistent with two possible disease mechanisms or a combina-

tion thereof: (i) an interrupted retinoid cycle that is potentially treatable by RPE65 gene replacement, RPE cell replacement, supplemental cis-retinoids, or any means to reestablish the biochemical pathway (1), and (ii) loss of photoreceptors, which would be more appropriate for therapeutic strategies such as visual prosthetics (41). The relative contributions of pure dysfunction and cell death to the extreme visual loss in human RPE65 deficiency are unknown. In a cohort of human retinal degeneration patients without RPE65 mutations, we used colocalized in vivo measures of function (by visual thresholds) and photoreceptor layer structure (by high-resolution cross-sectional optical imaging) and established the relationship of visual loss to cell loss. These data served as standards for comparison with similar results from individuals with RPE65 mutations. Human RPE65 disease did show a complex but interpretable structure–function relationship that differs not only from retinal degenerations not caused by RPE65 mutation but also from the disease stages in animal models when gene therapy was successful.

Our results for the cone-rich human fovea, a unique feature of primates, are without comparable data from murine and canine RPE65-mutant animals. Cone function, albeit severely impaired, was detected centrally in nearly half of the subjects with RPE65 mutations. Chromatic testing indicated that the function was indeed cone-mediated. Disproportionate preservation of foveal structure to a degree greater than expected for the level of foveal cone function (Fig. 3A) suggests an effect of RPE65 deficiency on human cones like that expected for rods. The exact role of RPE65 in relation to cones, however, may be more complex than that for rods (42, 43). The retinoid cycle of cones and rods has differences (44). RPE65, originally identified only in RPE, has also been found in cones of amphibians and in mammalian retina, including cow, rabbit, and mouse (43). Further complexity comes from a report of early cone degeneration in $Rpe65^{-/-}$ mice (45). Our findings suggest that human foveal cones may be more resistant to degeneration caused by RPE65 deficiency and thus most amenable to gene replacement therapy.

Rod photoreceptor topography in humans is not uniform, and there is a ring of highest rod density at ≈3–5 mm from the fovea (26). The rod/cone ratio in this region of human retina approximates that in murine and canine retina. Structure and function analyses in RPE65-deficient humans showed examples with no difference in function–structure pattern to other retinal degenerations, but there were also dramatic examples of greater ONL thickness than predicted from the level of impaired visual function. Graphs of ONL thickness as a function of retinal distance (Fig. 2E) suggest greatest preservation of the photoreceptor lamina at the region of highest rod density, i.e., 3- to 5-mm eccentricity (26). The region of reduced ONL thickness at lesser eccentricities resides on the "central flank of the rod ring" (26). A simple explanation for the shape of the ONL plots in RPE65-mutant retinas is that they represent cone and rod spatial densities. Peak ONL at the fovea reflects the peak spatial density of cones, which are retained in many RPE65-deficient retinas. The reduced ONL in extrafoveal retina may represent cone nuclei and/or a severely reduced spatial density of rods. The increased ONL thickness at 3- to 5-mm eccentricity, the site of the rod hot spot (26), suggests the presence of residual rod nuclei.

To return to the question of whether human RPE65-associated disease sufficiently resembles the animal models to warrant gene therapy in humans, the answer is in the affirmative but with caveats. In the adult RPE65-mutant retinas we studied, extrafoveal retinal regions with anatomical preservation would seem justifiable to treat. The implicit assumption is that measurable ONL has adjacent functional RPE (not measurable exclusive of other substructures by using OCT). The results of treatment of $Rpe65^{-/-}$ mice at advanced stages of disease were consistent with the hypothesis that degenerate retina would be treatable given enough retinal and RPE integrity. Our finding of variable

degrees of surviving photoreceptors at late disease stages in inherited retinal degeneration is not novel; other late-stage inherited retinal degenerations show similar variability (46). Far less success of gene therapy at later disease stages points to the intuitive notion that a thicker ONL would have more potential for functional recovery. A key concept from thickness topography and ONL measurements in these adult RPE65-deficient humans is that there was no straightforward relationship of age and amount of retinal degeneration.

Gene therapy targeted at the pericentral retina to restore rod (and cone) function and/or at the fovea to restore cone function thus seem worthy strategies, if pretreatment imaging studies indicate potential value of therapy. Focal intervention at exact retinal locations identified by pretreatment studies has been routine for many other retinopathies. For example, pretreatment angiography guides laser application to destroy abnormal subretinal angiogenesis and surgical removal of such vessels (47). Whether infants and children with *RPE65* mutations have less abnormal photoreceptor structure and require less pretreatment planning needs to be determined as human ocular gene therapy to restore vision progresses from a hopeful goal to an achievement.

1. Thompson, D. A. & Gal, A. (2003) *Prog. Retin. Eye Res.* **22,** 683–703.
2. Marlhens, F., Bareil, C., Griffoin, J. M., Zrenner, E., Amalric, P., Eliaou, C., Liu, S. Y., Harris, E., Redmond, T. M., Arnaud, B., *et al.* (1997) *Nat. Genet.* **17,** 139–141.
3. Gu, S. M., Thompson, D. A., Srikumari, C. R., Lorenz, B., Finckh, U., Nicoletti, A., Murthy, K. R., Rathmann, M., Kumaramanickavel, G., Denton, M. J., *et al.* (1997) *Nat. Genet.* **17,** 194–197.
4. Redmond, T. M., Yu, S., Lee, E., Bok, D., Hamasaki, D., Chen, N., Goletz, P., Ma, J. X., Crouch, R. K. & Pfeifer, K. (1998) *Nat. Genet.* **20,** 344–351.
5. Van Hooser, J. P., Aleman, T. S., He, Y. G., Cideciyan, A. V., Kuksa, V., Pittler, S. J., Stone, E. M., Jacobson, S. G. & Palczewski, K. (2000) *Proc. Natl. Acad. Sci. USA* **97,** 8623–8628.
6. Fan, J., Rohrer, B., Moiseyev, G., Ma, J. X. & Crouch, R. K. (2003) *Proc. Natl. Acad. Sci. USA* **100,** 13662–13667.
7. Gollapalli, D. R. & Rando, R. R. (2004) *Proc. Natl. Acad. Sci. USA.* **101,** 10030–10035.
8. Xue, L., Gollapalli, D. R., Maiti, P., Jahng, W. J. & Rando, R. R. (2004) *Cell* **117,** 761–771.
9. Acland, G. M., Aguirre, G. D., Ray, J., Zhang, Q., Aleman, T. S., Cideciyan, A. V., Pearce-Kelling, S. E., Anand, V., Zeng, Y., Maguire, A. M., *et al.* (2001) *Nat. Genet.* **28,** 92–95.
10. Narfstrom, K., Katz, M. L., Bragadottir, R., Seeliger, M., Boulanger, A., Redmond, T. M., Caro, L., Lai, C. M. & Rakoczy, P. E. (2003) *Invest. Ophthalmol. Visual Sci.* **44,** 1663–1672.
11. Dejneka, N. S., Surace, E. M., Aleman, T. S., Cideciyan, A. V., Lyubarsky, A., Savchenko, A., Redmond, T. M., Tang, W., Wei, Z., Rex, T. S., *et al.* (2004) *Mol. Ther.* **9,** 182–188.
12. Milam, A. H., Li, Z. Y. & Fariss, R. N. (1998) *Prog. Retin. Eye Res.* **17,** 175–205.
13. Machida, S., Kondo, M., Jamison, J. A., Khan, N. W., Kononen, L. T., Sugawara, T., Bush, R. A. & Sieving, P. A. (2000) *Invest. Ophthalmol. Visual Sci.* **41,** 3200–3209.
14. Bird, A. C., Farber, D. B., Kreiger, A. E., Straatsma, B. R. & Bok, D. (1998) *Invest. Ophthalmol. Visual Sci.* **29,** 2–11.
15. Porto, F. B., Perrault, I., Hicks, D., Rozet, J. M., Hanoteau, N., Hanein, S., Kaplan, J. & Sahel, J. A. (2002) *J. Gene Med.* **4,** 390–396.
16. Huang, Y., Cideciyan, A. V., Papastergiou, G. I., Banin, E., Semple-Rowland, S. L., Milam, A. H. & Jacobson, S. G. (1998) *Invest. Ophthalmol. Visual Sci.* **39,** 2405–2416.
17. Jacobson, S. G., Cideciyan, A. V., Aleman, T. S., Pianta, M. J., Sumaroka, A., Schwartz, S. B., Smilko, E. E., Milam, A. H., Sheffield, V. C. & Stone, E. M. (2003) *Hum. Mol. Genet.* **12,** 1073–1078.
18. Jacobson, S. G., Sumaroka, A., Aleman, T. S., Cideciyan, A. V., Schwartz, S. B., Roman, A. J., McInnes, R. R., Sheffield, V. C., Stone, E. M., Swaroop, A., *et al.* (2004) *Hum. Mol. Genet.* **13,** 1893–1902.
19. Lotery, A. J., Namperumalsamy, P., Jacobson, S. G., Weleber, R. G., Fishman, G. A., Musarella, M. A., Hoyt, C. S., Heon, E., Levin, A., Jan, J., *et al.* (2000) *Arch. Ophthalmol.* **118,** 538–543.
20. Roman, A. J., Schwartz, S. B., Aleman, T. S., Cideciyan, A. V., Chico, J. D., Windsor, E. A. M., Gardner, L. M., Ying, G., Smilko, E. E., Maguire, M. G., *et al.* (2005) *Exp. Eye Res.* **80,** 259–272.
21. Aleman, T. S., LaVail, M. M., Montemayor, R., Ying, G., Maguire, M. M., Laties, A. M., Jacobson, S. G. & Cideciyan, A. V. (2001) *Vision Res.* **41,** 2779–2797.
22. Van Hooser, J. P., Liang, Y., Maeda, T., Kuksa, V., Jang, G. F., He, Y. G., Rieke, F., Fong, H. K., Detwiler, P. B. & Palczewski, K. (2002) *J. Biol. Chem.* **277,** 19173–19182.
23. Maeda, T., Van Hooser, J. P., Driessen, C. A., Filipek, S., Janssen, J. J. & Palczewski, K. (2003) *J. Neurochem.* **85,** 944–956.
24. LaVail, M. M., Gorrin, G. M., Repaci, M. A., Thomas, L. A. & Ginsberg, H. M. (1987) *Invest. Ophthalmol. Visual Sci.* **28,** 1043–1048.
25. Chen, J., Simon, M. I., Matthes, M. T., Yasumura, D. & LaVail, M. M. (1999) *Invest. Ophthalmol. Visual Sci.* **40,** 2978–2982.
26. Curcio, C. A., Sloan, K. R., Kalina, R. E. & Hendrickson, A. E. (1990) *J. Comp. Neurol.* **292,** 497–523.
27. Rohrer, B., Goletz, P., Znoiko, S., Ablonczy, Z., Ma, J. X., Redmond, T. M. & Crouch, R. K. (2003) *Invest. Ophthalmol. Visual Sci.* **44,** 310–315.
28. Aleman, T. S., Jacobson, S. G., Chico, J. D., Scott, M. L., Cheung, A. Y., Windsor, E. A. M., Furushima, M., Redmond, T. M., Bennett, J., Palczewski, K., *et al.* (2004) *Invest. Ophthalmol. Visual Sci.* **45,** 1259–1271.
29. Bennett, J., Tanabe, T., Sun, D., Zeng, Y., Kjeldbye, H., Gouras, P. & Maguire, A. M. (1996) *Nat. Med.* **2,** 649–654.
30. Lewin, A. S., Drenser, K. A., Hauswirth, W. W., Nishikawa, S., Yasumura, D., Flannery, J. G. & LaVail, M. M. (1998) *Nat. Med.* **4,** 967–971.
31. Ali, R. R., Sarra, G. M., Stephens, C., Alwis, M. D., Bainbridge, J. W., Munro, P. M., Fauser, S., Reichel, M. B., Kinnon, C., Hunt, D. M., *et al.* (2000) *Nat. Genet.* **25,** 306–310.
32. Vollrath, D., Feng, W., Duncan, J. L., Yasumura, D., D'Cruz, P. M., Chappelow, A., Matthes, M. T., Kay, M. A. & LaVail, M. M. (2001) *Proc. Natl. Acad. Sci. USA* **98,** 12584–12589.
33. Morimura, H., Fishman, G. A., Grover, S. A., Fulton, A. B., Berson, E. L. & Dryja, T. P. (1998) *Proc. Natl. Acad. Sci. USA* **95,** 3088–3093.
34. Poehner, W. J., Fossarello, M., Rapoport, A. L., Aleman, T. S., Cideciyan, A. V., Jacobson, S. G., Wright, A. F., Danciger, M. & Farber, D. F. (2000) *Mol. Vis.* **6,** 192–198.
35. Thompson, D. A., Gyurus, P., Fleischer, L. L., Bingham, E. L., McHenry, C. L., Apfelstedt-Sylla, E., Zrenner, E., Lorenz, B., Richards, J. E., Jacobson, S. G., *et al.* (2000) *Invest. Ophthalmol. Visual Sci.* **41,** 4293–4299.
36. Lorenz, B., Gyurus, P., Preising, M., Bremser, D., Gu, S., Andrassi, M., Gerth, C. & Gal, A. (2000) *Invest. Ophthalmol. Visual Sci.* **41,** 2735–2742.
37. Hamel, C. P., Griffoin, J. M., Lasquellec, L., Bazalgette, C. & Arnaud, B. (2001) *Br. J. Ophthalmol.* **85,** 424–427.
38. Felius, J., Thompson, D. A., Khan, N. W., Bingham, E. L., Jamison, J. A., Kemp, J. A. & Sieving, P. A. (2002) *Arch. Ophthalmol.* **120** 55–61.
39. Yzer, S., van den Born, L. I., Schuil, J., Kroes, H. Y., van Genderen, M. M., Boonstra, F. N., van den Helm, B., Brunner, H. G., Koenekoop, R. K. & Cremers, F. P. (2003) *J. Med. Genet.* **40,** 709–713.
40. Lorenz, B., Wabbels, B., Wegscheider, E., Hamel, C. P., Drexler, W. & Preising, M. N. (2004) *Ophthalmology* **111,** 1585–1594.
41. Lakhanpal, R. R., Yanai, D., Weiland, J. D., Fujii, G. Y., Caffey, S., Greenberg, R. J., de Juan, E., Jr., & Humayun, M. S. (2003) *Curr. Opin. Ophthalmol.* **14,** 122–127.
42. Seeliger, M. W., Grimm, C., Stahlberg, F., Friedburg, C., Jaissle, G., Zrenner, E., Guo, H., Reme, C. E., Humphries, P., Hofmann, F., *et al.* (2001) *Nat. Genet.* **29,** 70–74.
43. Znoiko, S. L., Crouch, R. K., Moiseyev, G. & Ma, J. X. (2002) *Invest. Ophthalmol. Visual Sci.* **43,** 1604–1609.
44. Mata, N. L., Radu, R. A., Clemmons, R. S. & Travis, G. H. (2002) *Neuron* **36,** 69–80.
45. Crouch, R. K., Znoiko, S. L., Rohrer, B., Lu, K., Lohr, H. R. & Ma, J.-X. (2005) *Invest. Ophthalmol. Visual Sci.* **46,** 1473–1479.
46. LaVail, M. M., Matthes, M. T., Yasumura, D. & Steinberg, R. H. (1997) *Exp. Eye Res.* **65,** 45–50.
47. Ambati, J., Ambati, B. K., Yoo, S. H., Ianchulev, S. & Adamis, A. P. (2003) *Surv. Ophthalmol.* **48,** 257–293.
48. Simovich, M. J., Miller, B., Ezzeldin, H., Kirkland, B. T., McLeod, G., Fulmer, C., Nathans, J., Jacobson, S. G. & Pittler, S. J. (2001) *Hum. Mutat.* **18,** 164.
49. Al-Khayer, K., Hagstrom, S., Pauer, G., Zegarra, H., Sears, J. & Traboulsi, E. I. (2004) *Am. J. Ophthalmol.* **137,** 375–377.
50. Thompson, D. A., McHenry, C. L., Li, Y., Richards, J. E., Othman, M. I., Schwinger, E., Vollrath, D., Jacobson, S. G. & Gal, A. (2002) *Am. J. Hum. Genet.* **70,** 224–229.